Three-dimensional magnetic ordering in the quasi-one-dimensional Ising magnet $CoNb_2O_6$ with partially released geometrical frustration

S. Kobayashi and S. Mitsuda
Department of Physics, Faculty of Science, Science University of Tokyo, 1-3 Kagurazaka, Shinjuku-ku, Tokyo 162-8601, Japan

M. Ishikawa
Institute for Solid State Physics, University of Tokyo, Tokyo 106-8666, Japan

K. Miyatani
Department of Materials Science and Engineering, Ehime University, Matsuyama 790-8577, Japan

K. Kohn
School of Science and Engineering, Waseda University, Tokyo 169-8555, Japan
(Received 16 November 1998; revised manuscript received 9 February 1999)

The formation of three-dimensional magnetic ordering has been studied on a quasi-one-dimensional magnet $CoNb_2O_6$ by mean-field calculations as well as neutron scattering measurements down to $T=1.5$ K under magnetic fields up to $H_{\|c}\sim 600$ Oe. Measurements of a deviation of the magnetic Bragg scattering function from the delta function in the ordered state reveal a surprisingly rich variety of the magnetic formation arising from an isosceles triangular arrangement of the magnetic chain with competing interchain interactions in the a-b plane. The competing interactions result in quasidegenerate ground states with different propagation wave numbers along the b^* direction in the sinusoidally amplitude-modulated incommensurate magnetic (IC) phase. Our mean-field calculations qualitatively reproduce the complicated $H_{\|c}$-T magnetic phase diagram and give evidence for a high degeneracy of ground states by calculating the $H_{\|c}$-T dependence of the free energy curve in the propagation wave number space. In addition, a partial cancellation of the exchange field at the apex site from the base sites on the isosceles triangular lattice leads to a quasi-long-range ordering along the a axis in both IC and antiferromagnetic states where the correlation length along the a axis depends on the propagation wave number along the b^* direction. [S0163-1829(99)11121-4]

I. INTRODUCTION

Since in quasi-one-dimensional magnets weak interchain interactions extending in two directions lead the system to a three-dimensional (3D) magnetic ordered state, specific situations for interchain interactions cause an interesting formation of 3D magnetic ordering. For instance, when the system is geometrically frustrated due to a certain spatial arrangement of magnetic chains with competing interchain interactions, the system would exhibit diverse features such as incommensurate magnetic structure, complicated magnetic phase diagram, and a high degeneracy of ground states.[1] Particularly, if the geometrical frustration is partially released because of some distortion of competing interactions, there exists the possibility for appearing an unusual magnetic order absent in both frustrated and unfrustrated magnets.

Columbite $CoNb_2O_6$ may be an example of such a magnetic system. As shown in Fig. 1(a), Co^{2+} ions form 1D ferromagnetic zigzag chains along the orthorhombic c axis through 90°-Co^{2+}-O^{2-}-Co^{2+} superexchange interaction J_0. Because Co^{2+} ions arrange in an *isosceles triangular geometry* in the a-b plane, the magnetic chains can be considered to form the two-dimensional isosceles triangular lattice with the nearest-neighbor effective interchain exchange interaction J_1 and next-nearest-neighbor effective interchain exchange interaction J_2 in the a-b plane as shown in Fig. 1(b). Corresponding to the two crystallographically nonequivalent octahedral CoO_6 sites, there exist two different easy axes with a canting angle of $\pm\theta_0$ ($\sim 31°$) from the c axis. As indicated by the metamagnetism of this compound at $T=1.4$ K,[2] the system exhibits a pronounced Ising character at low temperatures. Since, as we will show later, J_1 and J_2 on the isosceles triangular lattice are antiferromagnetic and of similar magnitude, the system can be regarded as a triangular Ising antiferromagnet where the triangular geometrical frustration arising from the nearest-neighbor antiferromagnetic interaction is *partially* released along the b axis.

Early neutron diffraction measurements in zero field[3] revealed successive phase transitions at $T_1\sim 3.0$ K and $T_2\sim 1.9$ K: the incommensurate-magnetic (IC) ordering at T_1 with the temperature-dependent propagation wave vector $\mathbf{q}_{\rm propa}=(0\ q\ 0)$ and the noncollinear antiferromagnetic (AF) ordering at T_2 with $\mathbf{q}_{\rm propa}=(0\ 1/2\ 0)$. Recently, Hanawa *et al.* proposed an interesting $H_{\|c}$-T magnetic phase diagram where a field-induced spin-flop phase transition from the AF phase to the ferrimagnetic (FR) phase occurs below T_2.[4] They suggested that the FR structure has an up-up-down spin structure and revealed a low-dimensional magnetic character as well as the presence of competing exchange interactions in this compound.

Recently, we performed neutron scattering measurements in zero field[5,6] as well as under magnetic fields at $T=1.5$ K (Ref. 7) and found that the magnetic Bragg scattering func-

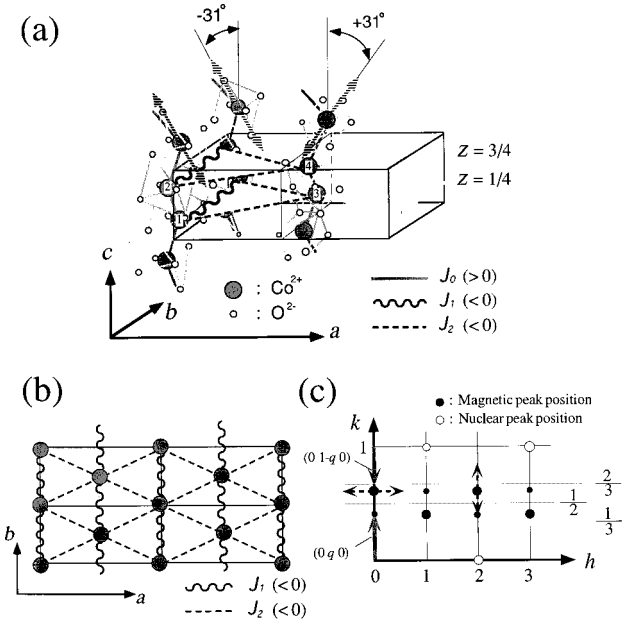

FIG. 1. (a) Schematic drawing of the ferromagnetic zigzag chains running along the c axis through the intrachain interaction J_0. The hatched arrows represent the two different easy axes. Co^{2+} ions occupy the $4(c)$ site in the space group *Pbcn* (No. 60) in the chemical unit cell: (1) $(0\, y_0\, 1/4)$, (2) $(0\, -y_0\, 3/4)$, (3) $(1/2\, 1/2\, +y_0\, 1/4)$, and (4) $(1/2\, 1/2-y_0\, 3/4)$ with $y_0=0.165$ (Ref. 8). (b) Isosceles triangular lattice with interchain antiferromagnetic interactions J_1 and J_2 in the a-b plane. (c) Schematic drawing of the reciprocal lattice in the $(h\, k\, 0)$ zone in the ordered state. The dashed arrows represent transverse scan directions. The peak positions schematically shown by large circles yield large intensity.

tion in the a^* and b^* directions perpendicular to the chain direction is not the delta function in both AF and IC phases. We observed a pronounced 2D character in the AF phase as the anisotropic broadening of the Lorentzian scattering function in the a^* direction and directly demonstrated that this results from an exact cancellation of the exchange field at the apex site from the base sites through J_2 on the isosceles triangular lattice. In addition, in the field-induced AF-FR phase transition, a quite broad magnetic response with field-dependent incommensurate propagation wave numbers between 1/3 and 1/2 along the b^* direction was observed. Correspondingly, an enhancement of the imaginary part in ac susceptibility was detected, which implies the existence of many metastable states, reflecting competing interchain interactions on the isosceles triangular lattice.

After these works were completed, we learned of another neutron diffraction study under magnetic fields by Heid *et al.*[8] They proposed a $H_{\|c}$-T magnetic phase diagram and indicated that the IC structure below T_1 in zero field is a sinusoidally amplitude-modulated structure. Nevertheless, the anomalous broadening of the scattering profile found in our studies was not studied in detail.

In this paper, we present results of further single-crystal neutron scattering measurements under magnetic fields on $CoNb_2O_6$ as well as results of mean-field calculations for the isosceles triangular lattice model with J_0, J_1, and J_2. These results reveal a surprisingly rich variety of magnetic formation in $CoNb_2O_6$ arising from the isosceles triangular arrangement of magnetic chains with competing interchain interactions. The competing interchain interactions result in a large number of quasidegenerate ground states with different propagation wave numbers along the b^* direction in the IC phase. Approaching the triple point where the AF, IC, and FR phases meet together, the degeneracy of ground states increases in the IC phase. In addition, owing to a partial cancellation of the exchange field at the apex site from the base sites on the isosceles triangular lattice, the system exhibits a quasi-long-range order along the a axis in both AF and IC phases where the magnetic correlations along the a axis are controlled by the difference in the magnitude of the base site spins. These results including our previous neutron scattering studies[5–7] are fully discussed.

In addition to the results for $CoNb_2O_6$, we also present results of single-crystal neutron scattering measurements on isomorphous compound $NiNb_2O_6$ where a weak Ising character of Ni^{2+} and exchange parameters different from those of $CoNb_2O_6$ may provide an interesting magnetic order. In recent powder neutron diffraction measurements,[9] Heid *et al.* observed antiferromagnetic ordering below $T_N \sim 5.9$ K and proposed that noncollinear AF structures with magnetic unit cell doubling of the chemical unit cell along both a and b axes coexist with the noncollinear AF structure with $\mathbf{q}_{\text{propa}} = (0\ 1/2\ 0)$. However, no single-crystal neutron scattering measurements in view of the deviation of the magnetic Bragg scattering function from the delta function have been made, although an exact cancellation of the exchange field at the apex site from antiparallel spins on the base sites implies the appearance of a pronounced 2D character as was observed in the AF phase in $CoNb_2O_6$. In this paper, neutron scattering results on single crystals of $NiNb_2O_6$ are also discussed in detail.

The rest of this paper is organized as follows. In Sec. II, we briefly describe experimental details. In Sec. III, which consists of five subsections (Secs. III A–III E), we present neutron scattering results as well as mean-field calculations on $CoNb_2O_6$. First, in Sec. III A, we confirm the one-dimensional character above T_1. We then determine the $H_{\|c}$-T magnetic phase diagram in Sec. III B and elucidate the quasi-3D magnetic behavior in the ordered state through scattering profile analysis in Sec. III C. In Sec. III D, the results of the mean-field calculations for the isosceles triangular lattice model are given. In Sec. III E, the pronounced 2D character found in the AF phase as well as the origin of the propagation wave number dependence of the correlation length along the a axis in the IC phase is discussed. In Sec. IV, we present the neutron scattering results on $NiNb_2O_6$ and compare these results with those of $CoNb_2O_6$. Finally, in Sec. V, we summarize our conclusions.

II. EXPERIMENT

The neutron scattering experiments on $CoNb_2O_6$ were performed at JRR-3M, in the Japan Atomic Energy Research Institute (JAERI) at Tokai, Japan, mainly using the triple-axis spectrometer (4G) in a two-axis mode. Second-order contamination was eliminated by a pyrolytic-graphite (PG) filter. The collimation with 40′-40′-40′-open and 40′-20′-20′-open from reactor to detector was employed. Incident neutrons with wave numbers 3.825 and 2.57 $Å^{-1}$ were used. The single crystal, to which we refer as sample

A_{Co}, with dimensions $3\times3\times7$ mm^3 was prepared by a flux growth technique.[10] The lattice parameters for the orthorhombic unit cell were determined to be $a=14.17$ Å, $b=5.71$ Å, and $c=5.04$ Å by neutron scattering measurements at $T=1.5$ K. The sample was mounted in a pumped ^{4}He cryostat with the $(h\,k\,0)$ or the $(0\,k\,l)$ scattering plane. For the measurements under magnetic fields, we selected the $(h\,k\,0)$ scattering plane with vertical external magnetic fields along the c axis up to 613 Oe. Part of the neutron scattering measurements in zero field presented in Sec. III E 3 was performed on single-crystal sample B_{Co} with dimensions $5\times5\times10$ mm^3, grown by a flux growth technique in a batch different from that for sample A_{Co}. We also performed magnetization measurements along the c axis down to $T=1.7$ K using a commercial dc superconducting quantum interference device (SQUID) magnetometer at Science University of Tokyo (Noda campus).

The neutron scattering experiments on isomorphous $NiNb_2O_6$ were carried out on the high-Q resolution triple-axis spectrometer (T1-1) in a two-axis mode, installed at JRR-3M. A PG filter was used to reduce second-order contaminant neutrons. The collimation from reactor to detector was open-60′-open, and the wave number of neutrons was 2.59 Å^{-1}. We used two single crystals with the same batch prepared by a flux growth technique: sample A_{Ni} with dimensions $2\times2\times12$ mm^3 and sample B_{Ni} with dimensions $1\times2\times8$ mm^3. Both samples were aligned with the $(h\,k\,0)$ plane horizontal and mounted in a pumped ^{4}He cryostat. From x-ray measurements using the powder specimen of crushed single crystals, the lattice parameters were determined to be $a=14.02(0)$ Å, $b=5.67(8)$ Å, and $c=5.01(9)$ Å, being in good agreement with the powder neutron diffraction data.[9]

III. RESULTS AND DISCUSSION FOR $CoNb_2O_6$

A. One-dimensional magnetic character above T_1

The one-dimensional magnetic character in $CoNb_2O_6$ above T_1 is provided by the strong interchain superexchange interaction along the orthorhombic c axis and by much weaker interchain interactions extending perpendicular to the chain. In neutron scattering measurements, the one dimensionality of the chain can be directly confirmed by observing the formation of magnetic Bragg planes perpendicular to the chain direction above the 3D ordering temperature. The location of the magnetic Bragg planes in the reciprocal lattice space reflects the type of magnetic chain: ferromagnetic or antiferromagnetic. Since as shown in Fig. 1(a) there exist Co^{2+} ions at both $z=1/4$ and 3/4 in the chemical unit cell and the magnetic structure in the ordered state indicates ferromagnetic interchain coupling,[3] we can expect the formation of magnetic Bragg planes at $l=$ even integer.

In order to elucidate a planar character of magnetic scattering above T_1, we performed scans along the a^*, b^*, and c^* directions above T_1 around the (0 0.62 0) IC peak position at $T\sim T_1$. As shown in Figs. 2(a)–2(c), in contrast to no appreciable magnetic scattering at $T=8.0$ K $(\sim2.7T_1)$, magnetic diffuse scattering was clearly observed at $T=4.0$ K$(\sim1.4T_1)$. The scattering profile along the c^* direction is very sharp compared with that along the a^* or

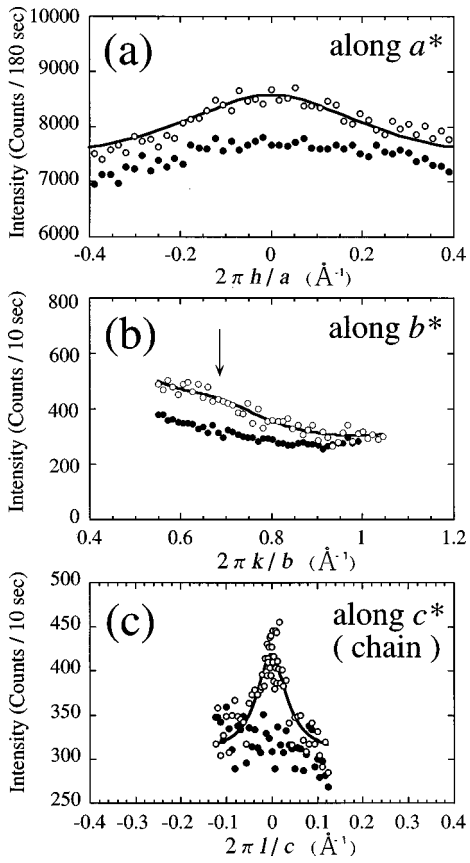

FIG. 2. Diffuse scattering along (a) a^*, (b) b^*, and (c) c^* directions around the (0 0.62 0) IC peak position at $T\sim T_1$ (solid arrow). The open and solid circles represent the intensity at $T=4.0$ and 8.0 K, respectively. The solid lines through the data at $T=4.0$ K show the least-squares fits to the Lorentzian with a correction for the background and magnetic form factors. Because of the direct neutron beam, a large background was observed at a lower scattering angle.

b^* direction, clearly showing the planar character of the magnetic scattering above T_1. Quantitatively, the least-squares fittings give the correlation length at $T=4.0$ K as $\xi_a\sim2.6$ Å, $\xi_b=3-6$ Å, and $\xi_c\sim26.3$ Å along the a, b, and c directions, respectively. The anisotropy in the correlation length indicates a quasi-1D magnetic character above T_1, being consistent with the low-dimensional character suggested by the magnetic specific heat above T_1.[4]

B. $H_{\|c}$-T magnetic phase diagram

Recently, Hanawa *et al.* proposed a $H_{\|c}$-T magnetic phase diagram shown in Fig. 3(a) (solid line).[4] The magnetic structure in the AF phase is noncollinear antiferromagnetic structure shown in Fig. 3(b),[3] while that in the FR phase has the up-up-down spin structure of Fig. 3(d).[4,7] Quite recently, Heid *et al.*[8] proposed a $H_{\|c}$-T magnetic phase diagram of Fig. 3(a) (dotted line) and suggested that the magnetic structure in the IC phase is the sinusoidally amplitude-modulated structure shown in Fig. 3(e); hereafter, we simply call this structure *sinusoidal structure*. However, there exist several discrepancies between the phase boundaries determined.

To determine the phase boundary, we investigated the magnetic-field dependence of the scattering profile of the

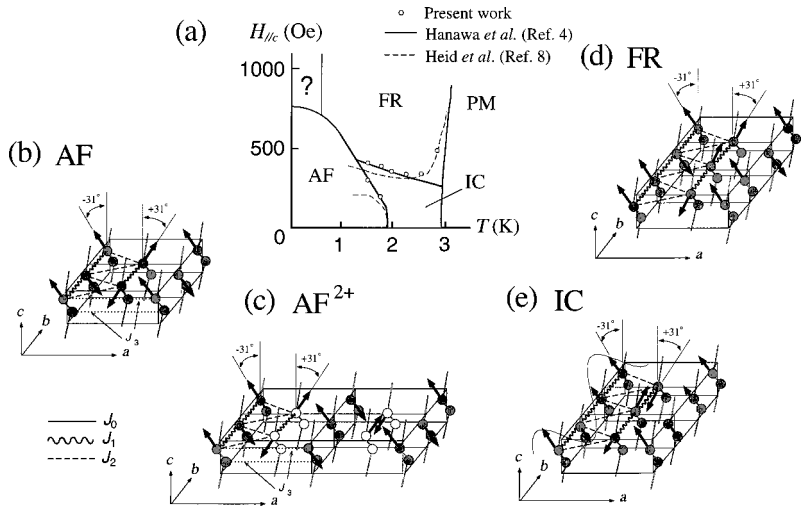

FIG. 3. (a) $H_{\|c}$-T magnetic phase diagram of $CoNb_2O_6$. The solid and dashed lines represent phase boundaries determined from Refs. 4 and 8, respectively. The shaded area shows the IC region determined from the present work (open circles). The question-marked area shows the region where a very complicated historical dependence on the metamagnetic behavior was detected in Ref. 4. (b) Noncollinear AF structure. (c) AF^{2+} domain structure which coexists with the AF structure (Sec. III E 3). The AF^{2-} domain is produced by reversing the spins shown by open circles. The dotted lines shown in the AF and $AF^{2\pm}$ structures represent the interchain interaction J_3 which shows up *only* in the AF phase. (d) Up-up-down FR structure and (e) sinusoidal structure in the IC phase.

$(2\,k\,0)$ transverse scan [Fig. 1(c)] at several temperatures below T_1. In the temperature range $T_2<T<T_1$, the IC Bragg peak appears in zero field as shown in Figs. 4(a)–4(d). With increasing magnetic field, the IC Bragg peak continuously shifts toward the FR position of $k=2/3$ and finally the first-order IC-FR phase transition occurs with a coexistence of both types of ordering. Below T_2, in addition, the AF Bragg peak appears in a lower-field region as shown in Figs. 4(e) and 4(f). Defining a critical field as the field where the integrated intensities of the successive phases are equal, we determined critical fields as shown in Fig. 3(a) (open circles). At lower temperatures, our data agree well with the results of Hanawa *et al.*[4] where the IC region surrounded by both AF-IC and IC-FR phase boundaries becomes narrower with decreasing temperature and these boundaries merge at a sufficiently low temperature, forming a triple point where the AF, IC, and FR phases meet together. On the other hand, at higher temperatures, a distinct increase of the IC-FR critical field was observed, being consistent with the neutron diffraction results[8] rather than the bulk results by Hanawa *et al.*[4] These features were also confirmed quite recently by our ac susceptibility measurements[11] and were qualitatively reproduced by our mean-field calculations for the isosceles triangular lattice model with J_0, J_1, and J_2 as will be shortly discussed in Sec. III D.

We here note the magnetic structure in the IC phase. Based on the powder results,[8] we confirmed that the sinusoidal structure well explains the observed intensity of our single-crystal neutron diffraction results at $T=2.84\,\mathrm{K}(q=0.385)$. At this temperature, no observable higher components were detected. When the temperature decreases, we found that higher harmonic peaks are gradually developed. Though an accurate magnetic structure at this temperature cannot be determined, the appearance of higher harmonics obviously suggests a deviation from the sinusoidal structure at lower temperature.

C. Quasi-three-dimensional behavior in ordered state

We now pay attention to a deviation of the magnetic Bragg scattering function from delta function in the ordered phase. In Fig. 5, we show the scattering profiles in the $(h\,1\,-q\,0)$ transverse scan at $T=1.5\,\mathrm{K}$ for each ordered state. As shown in Figs. 4 and 5(a), over the entire FR phase, the magnetic Bragg peak in both a^* and b^* directions is resolution-limited Gaussian, showing *true* 3D long-range ordering in the FR phase. However, in both AF and IC phases, an anomalous broadening of the scattering profile was detected. While in the IC phase the scattering profile along the a^* direction is sharp Lorentzian with a finite inverse correlation length as shown in Fig. 5(b), that along the b^* direction anisotropically broadens at low temperatures. On the other hand, in the AF phase the magnetic Bragg peak in the b^* direction is close to resolution-limited Gaussian as shown in Figs. 4(e) and 4(f), while that in the a^* direction is Lorentzian as shown in Fig. 5(c). Particularly, when the system is cooled rapidly from the higher-temperature IC state above T_2, we observed a broad Lorentzian scattering profile along the a^* direction with a low peak height.

In order to account for the deviation of the magnetic Bragg scattering function from the δ function in the ordered state quantitatively, we performed resolution-convoluted fits assuming the anisotropic functional form of

$$S(\mathbf{q})\propto\frac{\kappa}{\kappa^2+q_a^2}\exp\left[-\ln 2\left(\frac{q_b}{W_b}\right)^2\right]\exp\left[-\ln 2\left(\frac{q_c}{W_c}\right)^2\right] \quad (1)$$

as the magnetic Bragg scattering function instead of the delta function $\delta(\mathbf{q})$. Here $\mathbf{q}=(q_a\,q_b\,q_c)$ is a reciprocal lattice vector measured from the magnetic Bragg point. Fitting width parameters κ, W_b, and W_c are the half width at half maximum (HWHM) in the a^*, b^*, and c^* directions, respectively. For the Gaussian FR peak in the a^* direction, the Lorentzian term in Eq. (1) is replaced by

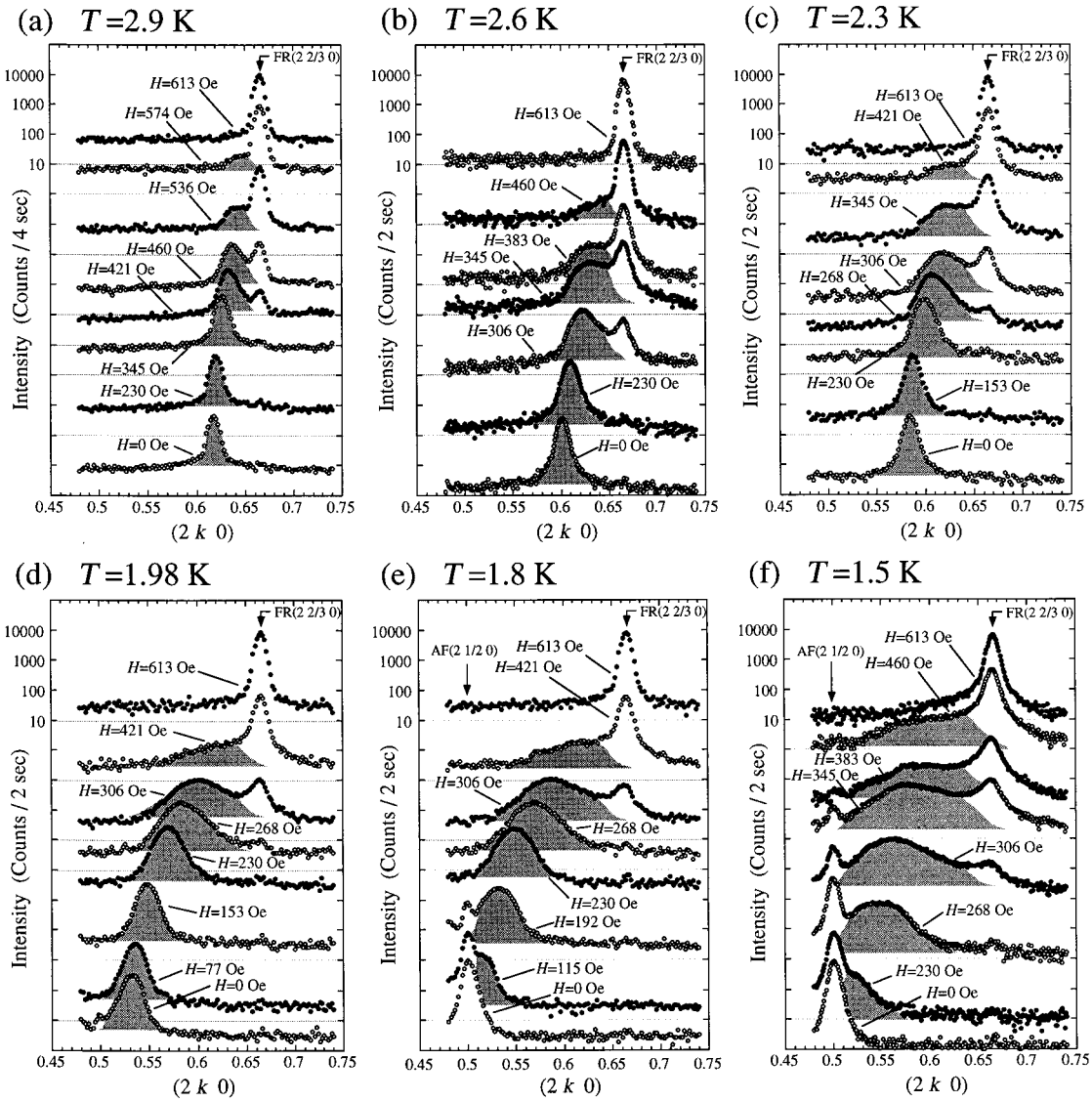

FIG. 4. Magnetic-field dependence of the scattering profile of the $(2\ k\ 0)$ transverse scan at (a) $T=2.9$ K, (b) $T=2.6$ K, (c) $T=2.3$ K, (d) $T=1.98$ K, (e) $T=1.8$ K, and (f) $T=1.5$ K. To clearly show the broadening of the scattering profile in the IC phase, the IC peaks are shaded.

$\exp[-\ln 2(q_a/W_a)^2]$ with a HWHM of W_a. Since both longitudinal and vertical resolutions are much wider than each width parameter, W_a and W_b were obtained from least-squares fits to experimental data with $S(\mathbf{q})$ convoluted with the transverse Gaussian resolution function. κ, which represents an inverse correlation length in units of $(2\pi/a)$, was obtained from 3D resolution-convoluted fits fixing W_c $(=0.0)$ and W_b. The resolution function around the magnetic Bragg points was determined by extrapolation from several nuclear Bragg peaks near the magnetic Bragg points.

In Figs. 6(a)–6(c), we show contour plots of the propagation wave number q and the width parameters κ and W_b on the $H_{\|c}$-T plane. To present the temperature dependence of the width parameters in zero field more clearly, it is also shown in Figs. 7(a)–7(c), together with κ and W_b in the AF state obtained after a rapid cooling down to $T=1.5$ K from the IC state. Over the FR phase, W_a^{FR} and W_b^{FR} are nearly zero and no deviation of the magnetic Bragg scattering function from the δ function was detected within our experimental accuracy. In both AF and IC phases, however, the magnetic Bragg scattering function in the a^* and b^* directions perpendicular to the chain is not the δ function. Both κ and W_b are quite small, but finite, indicating that the system is in a *quasi-3D magnetic ordered state*. As shown in Figs. 6(b) and 7(b), κ^{IC} in the IC phase increases monotonically approaching the AF-IC phase boundary. Particularly, comparing the $H_{\|c}$-T dependence of κ^{IC} with that of q shown in Fig. 6(a), κ^{IC} seems to depend on q. In addition, approaching the triple point in the IC phase, W_b^{IC} anomalously increases as shown in Fig. 6(c) and the width parameters become strongly anisotropic in the vicinity of the triple point: $W_b^{\mathrm{IC}}\sim 2.6\times 10^{-2}b^*$ and $\kappa^{\mathrm{IC}}\sim 1.8\times 10^{-3}a^*$ at $T=1.5$ K and $H_{\|c}=306$ Oe.

In contrast, in the AF phase both κ^{AF} and W_b^{AF} are weakly temperature and magnetic field dependent as shown in Figs. 6(b), 6(c) and 7(b), 7(c). However, for the rapid-cooling case, κ^{AF} yields a much higher value of $\sim 1.0\times 10^{-2}a^*$ at $T=1.5$ K as shown in Fig. 7(b), while W_b^{AF} remains to be nearly equilibrium value as shown in Fig. 7(c). This anisotropy in the width parameters found after rapid cooling indi-

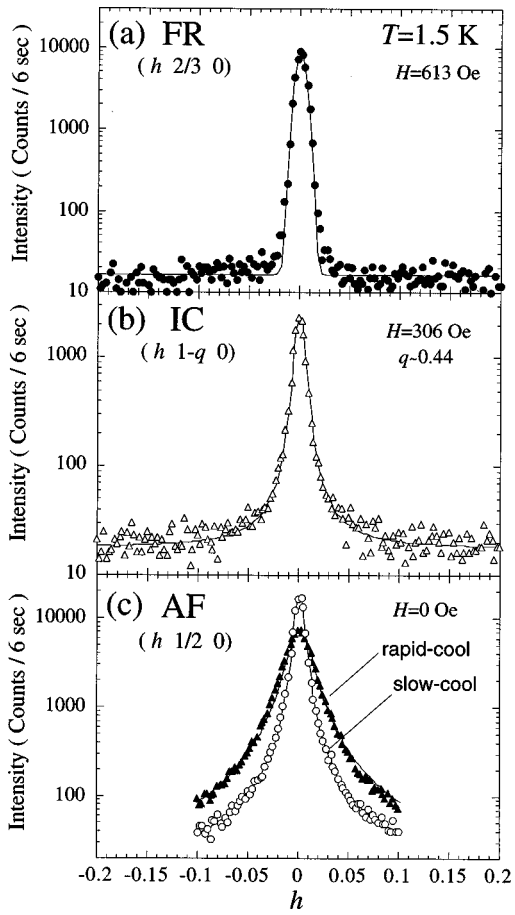

FIG. 5. Scattering profiles along the a^* direction at $T=1.5$ K under magnetic fields, measured at (a) FR (0 2/3 0), (b) IC (0 1 $-q$ 0), and (c) AF (0 1/2 0) peak positions. The scattering profile in the AF state just after rapid cooling from the IC state with a cooling rate of 0.05 K/sec is also shown (solid triangles).

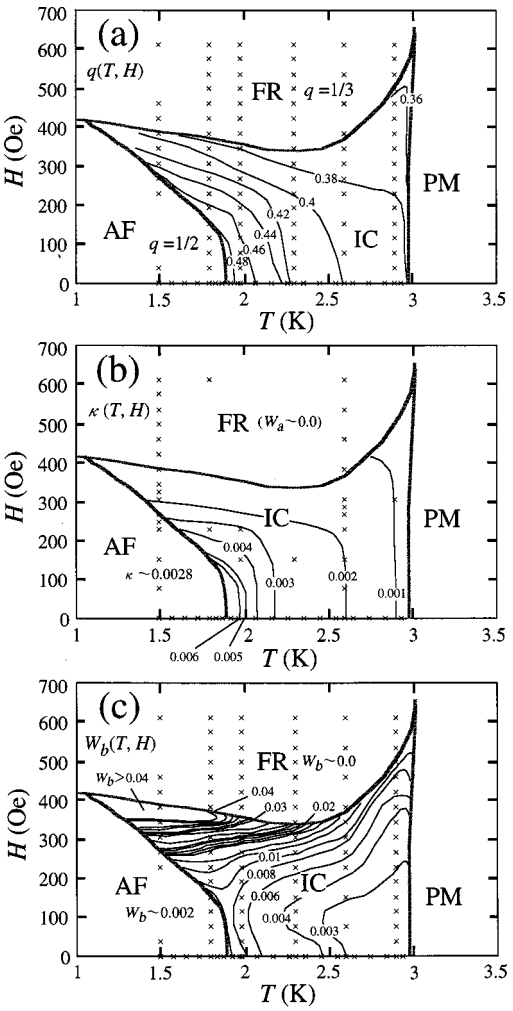

FIG. 6. (a) Contour plot of q on the $H_{\|c}$-T plane, determined from the magnetic peak position in the (2 k 0) scan. Contour plots of (b) κ and (c) W_b on the $H_{\|c}$-T plane. The location of measuring temperatures and magnetic fields is shown by crosses in the figures.

cates the appearance of a pronounced 2D magnetic character in the AF state.[5–7] When the temperature increases from $T=1.5$ K, κ^{AF} for the rapid-cooling case (rectangles) drastically decreases as it approaches equilibrium κ^{AF} (solid triangles). This means that rapid cooling produces nonequilibrium magnetic correlations along the a axis in the AF state and the anomalous decrease in κ^{AF} with increasing temperature is due to the relaxation behavior of nonequilibrium magnetic correlations with a help of a thermal fluctuation of spins. Actually, our recent preliminary neutron scattering measurements at $T=1.5$ K (Ref. 12) revealed long-time relaxation of the correlation length along the a axis after rapid cooling. Such (interplanar) magnetic correlations depending on cooling processes have been observed in the quasi-2D Ising antiferromagnet Rb_2CoF_4.[13]

As will be discussed later, such an anomalous $H_{\|c}$-T variation of the width parameters described above reflects competing interchain interactions on the isosceles triangular lattice. For later discussion, we summarize our experimental facts as follows.

EF(A). *True* 3D long-range ordering is established over the entire FR phase.

EF(B). Approaching the triple point where the AF, IC, and FR phases meet together, the IC peak in the b^* direction anisotropically broadens: $\kappa^{\mathrm{IC}}\sim 1.8\times10^{-3}a^*$, $W_b^{\mathrm{IC}}\sim 2.6\times10^{-2}b^*$ at $T=1.5$ K, and $H_{\|c}=306$ Oe (Sec. III D).

EF(C). In the AF state the correlation length along the a axis depends on the cooling speed from the higher-temperature IC state. In a case of rapid cooling from the IC state, the correlation length along the a axis becomes anisotropic and the system exhibits a pronounced 2D character (Sec. III E 1).

EF(D). In the IC phase the correlation length along the a axis depends on the propagation wave number q along the b^* direction. As q approaches 1/2, κ^{IC} increases monotonically (Sec. III E 2).

D. Interpretation of magnetic ordering by mean-field calculations

As is itemized as EF(B), in the vicinity of the triple point, the IC peak in the b^* direction anomalously broadens, while that in the a^* direction is quite sharp Lorentzian. This implies that the broad IC peak in the b^* direction is an assembly of a number of magnetic Bragg peaks with different propagation wave numbers between 1/3 and 1/2. Therefore, it is considered that the IC states with different propagation

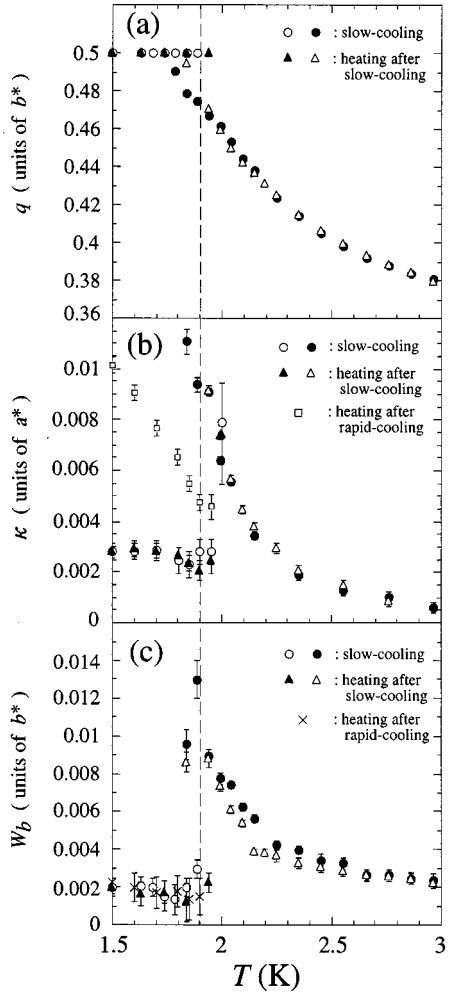

FIG. 7. Temperature dependence of (a) q, (b) κ, and (c) W_b in zero field. The dashed line represents the IC-AF transition temperature of $T_2 \sim 1.9$ K determined in increasing temperature. The rectangles and crosses show κ and W_b in the AF state obtained in increasing temperature after a rapid cooling down to $T = 1.5$ K.

wave numbers have nearly same free energies near the triple point. Taking account of the anomalous increase of W_b^{IC} shown in Fig. 6(c), it is most likely that the number of quasidegenerate ground states increases, approaching the triple point in the IC phase. In this subsection, we present results of mean-field calculations for the isosceles triangular lattice model with J_0, J_1, and J_2. We followed the mean-field studies for the Ising model of von Boehm and Bak[14] and calculated the propagation wave number dependence of the free energy curve in order to give evidence for the high degeneracy of ground states found in the IC phase.

1. Intrachain and interchain exchange parameters

First, we determine intrachain and interchain exchange parameters. As seen in the various magnetic structures shown in Figs. 3(b) and 3(d), 3(e), it is considered that the weak interchain exchange interactions J_1 and J_2 between the magnetic chains with intrachain coupling J_0 lead the system to the 3D ordered state. Thus, in the Ising approximation, the Hamiltonian of this system can be written as

$$\mathcal{H} = -J_0 \sum_{m,n,i,j} \mathbf{S}_{m,i} \cdot \mathbf{S}_{n,j} - J_1 \sum_{m,n,i,j} \mathbf{S}_{m,i} \cdot \mathbf{S}_{n,j} - J_2 \sum_{m,n,i,j} \mathbf{S}_{m,i} \cdot \mathbf{S}_{n,j} - g\mu_B \sum_{n,j} \mathbf{S}_{n,j} \cdot \mathbf{H}_{\mathrm{ex}}, \tag{2}$$

where $\mathbf{H}_{\mathrm{ex}}$ is an external magnetic field. $\mathbf{S}_{n,j}$ is the spin of the jth Co^{2+} ion ($j = 1-4$) in the nth chemical unit cell along the b axis and the summation is taken over pairs of spins.

Applying an external magnetic field along the c axis at low temperature below T_2, the system exhibits two field-induced phase transitions from the AF to the FR phase and from the FR to the saturated paramagnetic (PM) phase except the IC phase, which appears in a narrow field range. In the present magnetization measurements at $T = 1.7$ K, the critical fields of $H_c^{\text{AF-FR}} \sim 315$ Oe and $H_c^{\text{FR-PM}} \sim 3150$ Oe as well as the g value of ~ 2.1 with $S = 3/2$ are obtained. For three magnetically ordered phases, Eq. (2) yields energies at $T = 0$ K per Co^{2+} ion as

$$E_{\mathrm{AF}} = (-J_0 + J_1)S^2, \tag{3a}$$

$$E_{\mathrm{FR}} = \left(-J_0 + \frac{1}{3}J_1 + \frac{2}{3}J_2 \cos 2\theta_0\right)S^2 - \frac{1}{3}g\mu_B S H_{\parallel c} \cos\theta_0, \tag{3b}$$

$$E_{\mathrm{PM}} = (-J_0 - J_1 - 2J_2 \cos 2\theta_0)S^2 - g\mu_B S H_{\parallel c} \cos\theta_0. \tag{3c}$$

Since the level crossing between the energies of successive phases occurs at each critical field, we obtain following two equations:

$$g\mu_B S H_c^{\text{AF-FR}} \cos\theta_0 = (-2J_1 + 2J_2 \cos 2\theta_0)S^2, \tag{4a}$$

$$g\mu_B S H_c^{\text{FR-PM}} \cos\theta_0 = (-2J_1 - 4J_2 \cos 2\theta_0)S^2. \tag{4b}$$

Here Eqs. (4) contain only two parameters J_1 and J_2. Solving for J_1 and J_2 with $S = 3/2$ and $g = 2.1$, we obtain $J_1/k_B \sim -0.0508$ K and $J_2/k_B \sim -0.0812$ K.[15]

In Eqs. (4), J_0 does not appear explicitly, because the ferromagnetic spin arrangement along the chain remains in any ordered state. Thus we follow the mean-field approximation for the transition temperature in zero field[16] to determine J_0. In this approximation, the PM-IC transition temperature in zero field of $CoNb_2O_6$, T_1^{MF}, is expressed by

$$k_B T_1^{\mathrm{MF}} = (2J_0 + 2J_1 \cos 2\pi q^{\mathrm{MF}} - 4J_2 \cos 2\theta_0 \cos \pi q^{\mathrm{MF}})S^2, \tag{5}$$

where q^{MF} is the propagation wave number along the b^* direction at T_1^{MF} and is defined by

$$q^{\mathrm{MF}} = \frac{1}{\pi}\cos^{-1}\left(\frac{J_2 \cos 2\theta_0}{2J_1}\right). \tag{6}$$

Adopting the observed PM-IC transition temperature of $T_1 \sim 3.0$ K for T_1^{MF}, we obtain $J_0/k_B \sim 0.6015$ K. Note that the determined J_1 and J_2 give $q^{\mathrm{MF}} \sim 0.378$ through Eq. (6), which is consistent with our neutron scattering results of $q \sim 0.38$ at $T \sim T_1$.

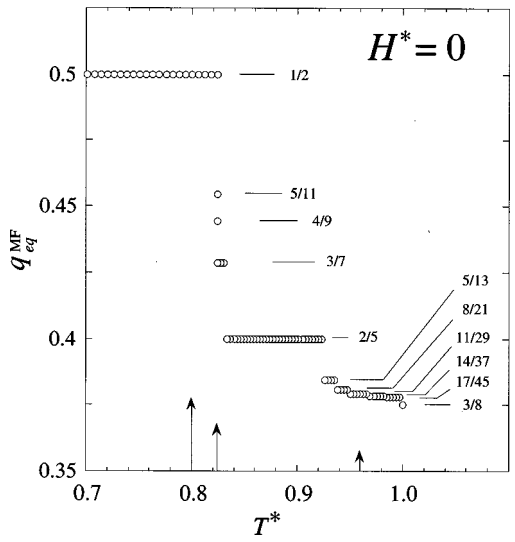

FIG. 8. Temperature dependence of the equilibrium propagation wave number $q_{\mathrm{eq}}^{\mathrm{MF}}$ in zero field.

2. Theory of mean-field calculation

In the mean-field approximation, the Hamiltonian of Eq. (2) is written as

$$\mathcal{H}^{\mathrm{MF}}=\frac{1}{2}g\mu_B\sum_{n,j}\mathbf{H}_{n,j}^{\mathrm{MF}}\cdot\hat{\mathbf{u}}_j\langle S_{n,j}\rangle-g\mu_B\sum_{n,j}(\mathbf{H}_{n,j}^{\mathrm{MF}}+\mathbf{H}_{\mathrm{ex}})\cdot\mathbf{S}_{n,j}. \tag{7}$$

The summation is taken over all spins. $\hat{\mathbf{u}}_j$ is a unit vector along the easy axis of the jth Co^{2+} ion, and $\langle S_{n,j}\rangle$ is a thermal average of the magnitude of spin $\mathbf{S}_{n,j}$. $\mathbf{H}_{n,j}^{\mathrm{MF}}$ is the effective exchange field acting on $\mathbf{S}_{n,j}$, which is expressed by

$$\mathbf{H}_{n,j}^{\mathrm{MF}}=\frac{1}{g\mu_B}\left(J_0\sum_{m,i}\langle S_{m,i}\rangle\hat{\mathbf{u}}_i+J_1\sum_{m,i}\langle S_{m,i}\rangle\hat{\mathbf{u}}_i+J_2\sum_{m,i}\langle S_{m,i}\rangle\hat{\mathbf{u}}_i\right). \tag{8}$$

The thermal average of the magnitude of $\mathbf{S}_{n,j}$ can be calculated from the relation

$$\langle S_{n,j}\rangle=S\tanh\left[\frac{g\mu_B S(\mathbf{H}_{n,j}^{\mathrm{MF}}+\mathbf{H}_{\mathrm{ex}})\cdot\hat{\mathbf{u}}_j}{k_BT^{\mathrm{MF}}}\right]. \tag{9}$$

Since the spins align ferromagnetically along both a and c axes in any ordered state, we considered a magnetic cell with dimensions $a\times Nb\times c$, where N is the number of chemical unit cells along the b axis. In this system, the periodic boundary condition was imposed: $\mathbf{S}_{n,j}=\mathbf{S}_{n+N,j}$. Therefore, the possible propagation wave number q^{MF} characterizing the spin configuration is strongly restricted to a rational value of n/N with $n=$integer.

A magnetic field was applied along the c axis. As an initial spin state, the sinusoidal structure with $q_{\mathrm{initial}}^{\mathrm{MF}}$ $(=n/N)$ or the self-consistent solution obtained at nearby temperature and magnetic field was employed. This spin state was used to calculate the effective exchange field at all spin sites by Eq. (8). This effective field as well as a magnetic field yields a new spin state through Eq. (9). These

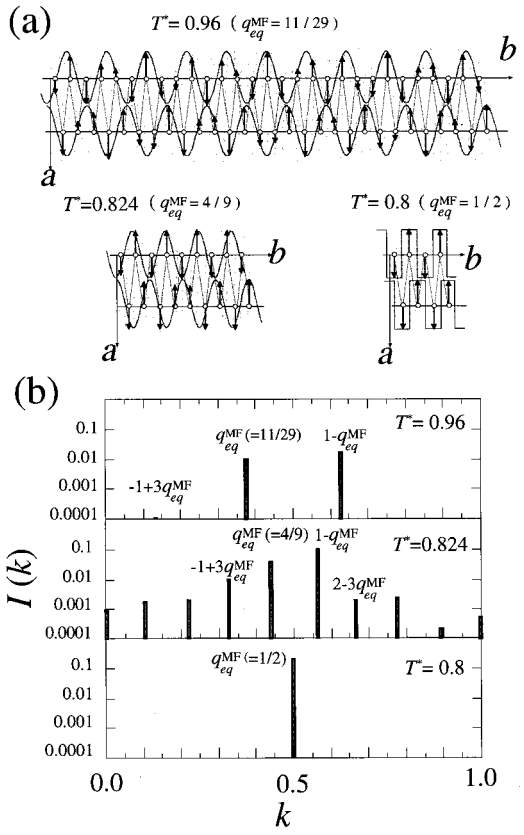

FIG. 9. (a) Spin arrangements on the isosceles triangular lattice in zero field at several temperatures. The shaded area corresponds to a magnetic unit cell. To illustrate the arrangement of spins along the b axis, the projection of the spins on the a-b plane at $z=1/4$ is drawn. The temperatures shown in the figures correspond to those indicated by the solid arrows in Fig. 8. (b) Calculated Fourier spectrum for these spin arrangements.

calculations were iterated until self-consistency was obtained. Then, for a final spin state, we calculated the free energy per spin $F(T^{\mathrm{MF}},H_{\|c})$ and a space Fourier transform of spins $I(k)$, using the following equations:

$$F(T^{\mathrm{MF}},H_{\|c})=-\frac{k_BT^{\mathrm{MF}}}{4N}\sum_{n=1}^{N}\sum_{j=1}^{4}\times\ln\left\{\mathrm{Tr}_{n,j}\left[\exp\left(-\frac{\mathcal{H}^{\mathrm{MF}}}{k_BT^{\mathrm{MF}}}\right)\right]\right\}, \tag{10}$$

$$I(k)=\left|\frac{1}{N}\sum_{n=1}^{N}\sum_{j=1}^{4}\mathbf{S}_{n,j}\exp(2\pi iky_{n,j})\right|^2. \tag{11}$$

Here $\mathrm{Tr}_{n,j}$ in Eq. (10) represents the trace over the two spin states for $\mathbf{S}_{n,j}=\pm S\hat{\mathbf{u}}_j$. k and $y_{n,j}$ in Eq. (11) are the wave number in the b^* direction and the coordinate of $\mathbf{S}_{n,j}$ in the b direction, respectively. The Fourier spectrum $I(k)$ can be compared directly with the observed magnetic structure factors in neutron scattering measurements. In our calculations, spins in the chain were ferromagnetic and of an equal magnitude for any final spin state, reflecting the strong intrachain ferromagnetic coupling J_0: $\mathbf{S}_{n,1}=\mathbf{S}_{n,2}$ and $\mathbf{S}_{n,3}=\mathbf{S}_{n,4}$. However, we found that the spin arrangement along the b axis in the final spin state depends strongly on the initial spin

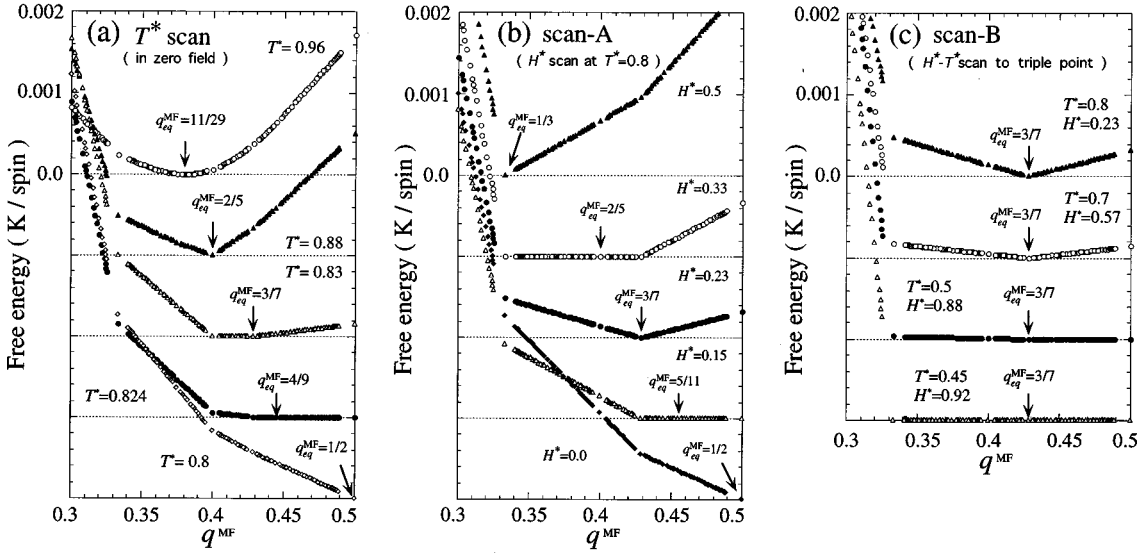

FIG. 10. Variation of the calculated free energy curve per spin as a function of q^{MF} (a) in zero field, (b) under magnetic fields at $T^*=0.8$ below T_2^* (scan A), and (c) with the approach to the triple point (scan B). The lowest free energy for each free energy curve is set to zero.

state at most locations surveyed on the $H_{\|c}$-T^{MF} magnetic phase diagram; an exception was the temperature just below T_1^{MF} and the magnetic field larger than $H_{\|c}\sim H_c^{\mathrm{FR\text{-}PM}}$. During the numerical iterations, the propagation wave number q^{MF} characterizing spin state by no means differed from $q_{\mathrm{initial}}^{\mathrm{MF}}$. Only higher-order components relative to the fundamental one in $I(k)$ varied after the iterative procedure. Because our model includes competing interactions J_1 and J_2, it may be difficult to generate another final spin state with a periodicity different from that of the initial one within the mean-field approximation ignoring the thermal fluctuation of spins. Nevertheless, we regarded the resultant final spin state as the spin state which minimizes the free energy at $q^{\mathrm{MF}}(=q_{\mathrm{initial}}^{\mathrm{MF}})$ in the F-q^{MF} space under the restriction that the characteristic propagation wave number be fixed during the iterations.

The mean-field calculations were performed with N up to 45. We selected $q_{\mathrm{initial}}^{\mathrm{MF}}$ between 0.3 and 0.5 and chose the spin state with the smallest N among initial spin states whose $q_{\mathrm{initial}}^{\mathrm{MF}}$ has an equal magnitude. Thus we could calculate 127 initial spin states with different $q_{\mathrm{initial}}^{\mathrm{MF}}$ and could obtain free energies for various different q^{MF}. Since the final spin state with the lowest free energy is stabilized, the equilibrium propagation wave number $q_{\mathrm{eq}}^{\mathrm{MF}}$ was readily determined from the F-q^{MF} curve obtained. The resultant F-q^{MF} curve provides important information about how metastable spin states are distributed around the equilibrium spin state with $q_{\mathrm{eq}}^{\mathrm{MF}}$ at a given $H_{\|c}$ and T^{MF}. Then, using final spin states at nearby the temperature and magnetic field as initial states, we surveyed the temperature and magnetic-field dependence of the F-q^{MF} curve and determined the $H_{\|c}$-T^{MF} magnetic phase diagram. For later discussion, we introduce reduced temperature T^* $(=T^{\mathrm{MF}}/T_1^{\mathrm{MF}})$ and reduced magnetic field H^* $(=H_{\|c}/H_c^{\mathrm{AF\text{-}FR}})$.

3. Zero field

In Fig. 8, we show the temperature dependence of $q_{\mathrm{eq}}^{\mathrm{MF}}$ in zero field. As the temperature decreases from the PM state, the IC state with $q_{\mathrm{eq}}^{\mathrm{MF}}=3/8$ $(=0.375)$ appears at $T^*=T_1^*$ $(=1.0)$. As seen in the spin configuration at $T^*=0.96$ shown in Fig. 9(a), the magnetic structure just below T_1^* is sinusoidal and no significant higher-order components were observed in $I(k)$ as shown in Fig. 9(b). With decreasing T^*, $q_{\mathrm{eq}}^{\mathrm{MF}}$ approaches 1/2 with a shift of the bottom of the F-q^{MF} curve as shown in Fig. 10(a). Correspondingly, the magnetic structure gradually deviates from the sinusoidal structure to a squared-up modulated one, yielding pronounced higher-order components in $I(k)$. As T^* decreases further, $q_{\mathrm{eq}}^{\mathrm{MF}}$ locks into 1/2 at $T^*=T_2^*$ (~ 0.82) and the AF structure with $q_{\mathrm{eq}}^{\mathrm{MF}}=1/2$ shown in Fig. 9(a) is stable down to $T^*=0$. These results are consistent with our neutron scattering results of the temperature variation of q [Fig. 7(a)] as well as the appearance of the higher harmonics just above T_2 (Sec. III B).

In addition, as shown in Fig. 10(a), we found that the bottom of the F-q^{MF} curve becomes flat around $q_{\mathrm{eq}}^{\mathrm{MF}}$ $(=4/9)$ at $T^*=0.824$ just above T_2^*. Correspondingly, as shown in Fig. 7(c), the anomalous increase of W_b along the direction of the propagation wave number was clearly observed just above T_2. This fact implies that the increase of W_b^{IC} just above T_2 is related to the flatness of the F-q^{MF} curve around $q_{\mathrm{eq}}^{\mathrm{MF}}$. With these calculation data in hand, we proceed to the results for finite magnetic fields.

4. Magnetic field parallel to the c axis

In Fig. 11, we show the calculated H^*-T^* magnetic phase diagram. Our calculations qualitatively reproduce the $H_{\|c}$-T magnetic phase diagram of $CoNb_2O_6$, which consists of three magnetically ordered phases: AF, IC, and FR phases. The IC phase contains various magnetic states characterized by a rational value of $q_{\mathrm{eq}}^{\mathrm{MF}}$ between 1/3 and 1/2.[17] At both lower and higher temperatures, an increase in the IC-FR critical field is seen as was experimentally found in the present neutron scattering study [Fig. 3(a)]. The IC region, surrounded by both AF-IC and FR-IC phase boundaries, becomes narrower with decreasing temperature. Within

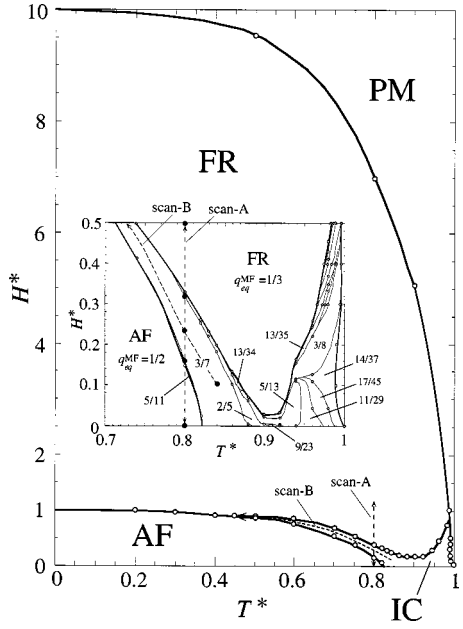

FIG. 11. Calculated H^*-T^* magnetic phase diagram. The inset shows its enlargement around the IC phase.

an accuracy of our mean-field calculations, these phase boundaries merge at $H^* \sim 0.96$ and $T^* \sim 0.4$, forming a triple point where the AF, IC, and FR phases meet together. Quite recent mean-field calculations for the axial-next-nearest-neighbor Ising (ANNNI) model on the tetragonal lattice[18] also provided a complicated H-T magnetic phase diagram similar to that found in our study. Noted that although in our calculations different H^*-T^* paths on the H^*-T^* plane yielded slightly different F-q^{MF} curves at given H^* and T^*, we found that such different F-q^{MF} curves substantially do not alter the resultant features described above.

We here consider two types of scan shown by dashed arrows in Fig. 11 in order to investigate the relation between W_b and the flatness of the F-q^{MF} curve around $q_{\mathrm{eq}}^{\mathrm{MF}}$: the H^* scan at $T^*=0.8$ below T_2^* (scan A) and the H^*-T^* scan to the triple point (scan B). As seen in the F-q^{MF} curve in scan A shown in Fig. 10(b), the bottom of the F-q^{MF} curve is quite deep around $q_{\mathrm{eq}}^{\mathrm{MF}}$ in both AF and FR states, while not in the IC phase. Particularly, near the AF-IC and IC-FR phase boundaries in the IC phase, the flatness of the F-q^{MF} curve around $q_{\mathrm{eq}}^{\mathrm{MF}}$ becomes pronounced. These results are consistent with the fact that the broadening of the scattering profile along the b^* direction was detected *not* in the AF and FR phases, but *only* in the IC phase. Furthermore, as shown in Fig. 10(c), the F-q^{MF} curve around $q_{\mathrm{eq}}^{\mathrm{MF}}$ gradually becomes flat approaching the triple point in the IC phase. At $T^*=0.45$ and $H^*=0.92$ in the vicinity of the triple point, a large number of spin states with different propagation wave numbers between 1/3 and 1/2 are nearly degenerated. This enhancement of a degeneracy of ground states might give rise to an increase in the number of IC Bragg peaks with different propagation wave numbers and therefore might cause a broadening of the IC peak along the b^* direction. Actually, approaching the triple point, W_b^{IC} anomalously increases as shown in Fig. 6(c).

In order to seek the presence of an assembly of IC Bragg peaks with different propagation wave numbers, we performed transverse scans along the b^* direction with high-Q resolution neutron scattering just above T_2 in zero field and also at $T=1.5$ K and $H_{\|c}=306$ Oe near the triple point. As shown in Fig. 12(a), the IC peak in the b^* direction just above T_2 is not a broad single peak, but peaks separated into two broad peaks. With decreasing temperature slightly from 1.98 K toward 1.92 K, these two peaks gradually broaden, accompanying a shift of their positions. Moreover, in the vicinity of the triple point, the IC peaks in the b^* direction are fairly rugged as shown in Fig. 12(b). Such fine structure of the magnetic scattering function directly evinces the presence of quasidegenerate ground states with different propagation wave numbers in the IC phase.

Corresponding to these neutron scattering results, our recent ac susceptibility measurements[11] revealed a low-frequency enhancement in χ'' only in the IC phase near the triple point. This slow dynamics probably reflects the existence of such quasidegenerate ground states. A detailed discussion of ac susceptibility measurements will be presented soon.

E. 2D character in a 3D ordered state

As is itemized as EF(C) and EF(D), the correlation length along the a axis varies depending on the propagation wave number along the b^* direction. In the AF phase in particular, the correlation length along the a axis depends on the cooling speed from the higher-temperature IC state and the system exhibits a pronounced 2D character when the system is

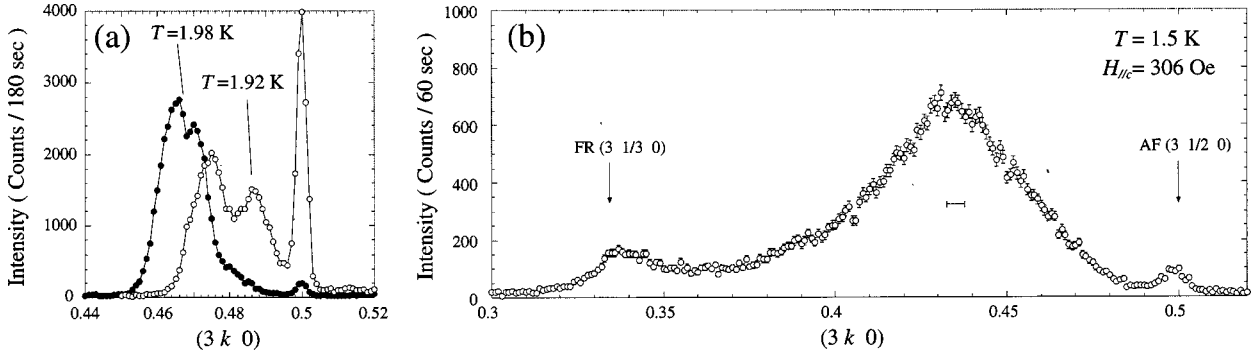

FIG. 12. Scattering profiles of the $(3\ k\ 0)$ transverse scan with high-Q resolution neutron scattering at (a) $T=1.92$ and 1.98 K in zero field and (b) at $T=1.5$ K and $H_{\|c}=306$ Oe near the triple point. The horizontal bar denotes the full width at half maximum of the resolution function at the IC peak position of $k \sim 0.435$.

cooled rapidly toward the AF state. In this subsection, we discuss the origin of the pronounced 2D character in the AF state (Sec. III E 1) and give an explanation for the $H_{\|c}$-T variation of κ^{IC} in the IC phase (Sec. III E 2). Then, in Sec. III E 3, we present a detailed discussion of the existence of antiferromagnetic domains closely relating to the 2D character in the AF phase.

1. 2D character in the AF phase

First, we show the origin of the pronounced 2D character in the AF phase within the isosceles triangular lattice model with J_1 and J_2. As seen in the AF structure of Fig. 3(b), spins confined along the easy axes are antiferromagnetically aligned along the *b* axis. Consequently, the exchange field at the apex site from the base sites through J_2 on the isosceles triangular lattice exactly cancels and the 2D magnetic sheets consisting of the magnetic chains anisotropically coupled along the *b* axis through J_1 are formed effectively. Thus, when the system is cooled rapidly toward the AF state, there may remain a number of stacking disorder between 2D magnetic sheets. Such a stacking disorder results in an anisotropic broadening of the Lorentzian magnetic Bragg scattering function in the a^* direction and is considered to be responsible for the dependence of the correlation length along the *a* axis on the cooling speed [Fig. 5(c)]. If such a situation actually takes place in $CoNb_2O_6$, the correlation length is expected to vary as the magnitude of the exchange field acting on the apex site varies. Indeed, in the spin-flop FR phase where one-third of the exchange field through J_2 *partially* recovers, the correlation length along the *a* axis dramatically increases as indicated by the resolution-limited FR peak along the a^* direction shown in Fig. 5(a).[7]

So far, we have treated this system as an isosceles triangular lattice model with J_1 and J_2. However, within this model, the observed κ^{AF} must be infinite and the system behaves as an ideal 2D magnetic system in the AF phase, because the exchange field between adjacent 2D magnetic sheets is exactly zero. Thus the magnetic peaks should be observed as a form of *rods* running along the a^* direction rather than *Bragg points* in the reciprocal lattice space as was observed in 2D antiferromagnets such as K_2NiF_4.[19] Taking account of the quasi-3D magnetic behavior in the AF state, a weak but finite effective interchain interaction J_3 illustrated by dotted lines in Fig. 3(b) is considered to stabilize the magnetic ordering along the *a* axis in the AF state. In fact, as will be shortly discussed in Sec. III E 3, owing to the existence of inhomogeneity in J_3, AF domains with different stacking of the 2D magnetic sheets along the *a* axis are realized *only* in the AF phase.

Even for the slow-cooling treatment, the quasi-3D magnetic behavior remains in the AF state. Recently, Hanawa *et al.* observed a small anomaly of the magnetic specific heat at a quite low temperature of ~ 0.65 K.[4] The appearance of such an anomaly probably means that the system goes into the *true* 3D long-range AF state at this temperature. In this case, the resolution-limited AF Bragg peak should be observed. Neutron scattering experiments down to $T=0.3$ K are now in planning in order to confirm the true 3D long-range antiferromagnetism below $T\sim 0.65$ K.

2. $H_{\|c}$-T variation of correlation length in the IC phase

In contrast to the case of the AF phase, in the IC phase the exchange field at the apex site from the base sites is not canceled exactly as shown in Fig. 3(e) owing to the difference in the magnitude of the sinusoidal spins on the base sites. Since such a difference reduces as q approaches 1/2, it is most likely that the inverse correlation length κ^{IC} increases as q approaches 1/2 as is itemized as EF(D).

To account for the $H_{\|c}$-T variation of κ^{IC} semiqualitatively, we assumed that the long-range IC ordering with q is established along the *b* axis and the 2D magnetic sheets thus formed correlate each other *one dimensionally* with κ^{IC} along the *a* axis through the effective interplanar nearest-neighbor interaction $J'_{\mathrm{effect}}(q)$. This treatment may be adequate, because the observed magnetic scattering function in the a^* direction is Lorentzian, which is the magnetic scattering function of the 1D model.[20] $J'_{\mathrm{effect}}(q)$ was determined by averaging effective exchange interactions between adjacent 2D magnetic sheets, using the following equation:

$$J'_{\mathrm{effect}}(q)=\frac{\Sigma_n|J'_n(q)|}{\Sigma_n 1}, \tag{12}$$

where

$$J'_n(q)=J_2\frac{\mathbf{S}_{n,1}(\mathbf{S}_{n,3}+\mathbf{S}_{n-1,3})}{S^2}. \tag{13}$$

Here $J'_n(q)$ is an exchange interaction acting on $\mathbf{S}_{n,1}$ at the apex site from two base site spins $\mathbf{S}_{n,3}$ and $\mathbf{S}_{n-1,3}$ on an isosceles triangle. Since the magnitude of $J'_n(q)$ differs from site to site due to the incommensurate spin arrangement along the *b* axis, the summation in Eq. (12) was taken over n up to 1000. For simplicity, we ignored the interchain interaction J_3 and a deviation from the sinusoidal structure. Since the inverse correlation length is a monotone decreasing function of an exchange parameter divided by temperature,[20] we surveyed the $H_{\|c}$-T dependence of $J'_{\mathrm{effect}}(q(T,H))/T$ and interpreted the $H_{\|c}$-T variation of κ^{IC} as below.

First, we show the temperature dependence of $J'_{\mathrm{effect}}(q(T))/T$ in zero field in the inset in Fig. 13. For comparison, the temperature dependence of $J'_{\mathrm{effect}}(q=0)/T$ is also plotted; for $q=0$, no interplanar exchange interaction cancels and $J'_{\mathrm{effect}}(0)$ $(=2J_2\cos 2\theta_0)$ is temperature independent. As is evident, in the case of $q=0$, $J'_{\mathrm{effect}}(0)/T$ increases monotonically with decreasing temperature. This means that the temperature-independent exchange interaction always develops magnetic correlations at low temperature. On the other hand, taking account of the temperature-dependent propagation wave number $q(T)$ in $CoNb_2O_6$, $J'_{\mathrm{effect}}(q(T))/T$ gradually decreases with decreasing temperature and becomes zero below T_2. Moreover, as shown in Fig. 13, approaching the IC-AF phase boundary, $J'_{\mathrm{effect}}(q(T,H))/T$ decreases in the IC phase. Considering the anomalous increase in κ^{IC} approaching the IC-AF boundary shown in Fig. 6(b), these calculations qualitatively evince that the difference in the magnitude of the base site spins controls the magnetic correlations along the *a* axis in the IC phase.

In these calculations we have assumed a long-range sinusoidal structure with q. However, in real system various fac-

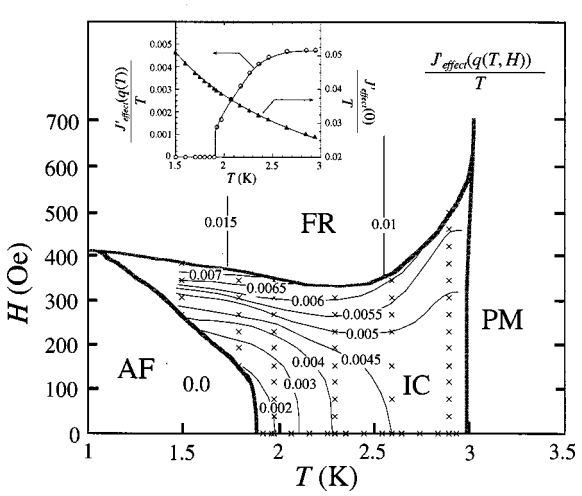

FIG. 13. Contour plot of $J'_{\text{effect}}(q(T,H))/T$ on the $H_{\|c}$-T plane, calculated from the observed $q(T,H)$ shown in Figs. 6(a) and 7(a). The crosses represent locations where $J'_{\text{effect}}(q(T,H))/T$ was calculated. The inset shows temperature dependence of $J'_{\text{effect}}(q=0)/T$ (triangles) and $J'_{\text{effect}}(q(T))/T$ (open circles) in zero field.

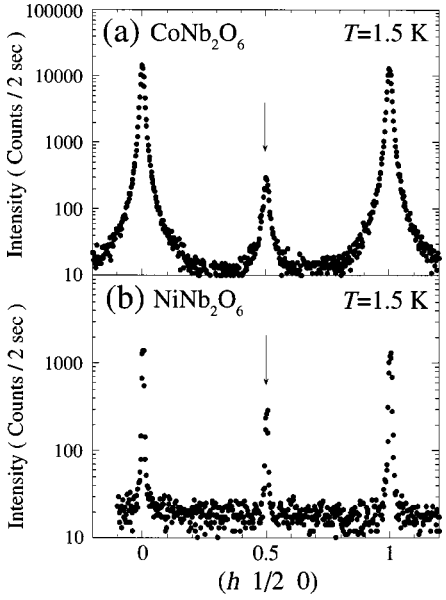

FIG. 14. Magnetic reflection in the $(h\ 1/2\ 0)$ scan at $T=1.5$ K in the AF state (a) for sample B_{Co} of $CoNb_2O_6$ and (b) for sample A_{Ni} of $NiNb_2O_6$. The additional AF peaks observed at $h=$ half-odd integer are depicted by solid arrows.

tors, such as a deviation from the sinusoidal structure due to an external field and the existence of quasidegenerated ground states, contribute to the magnetic correlations along the a axis; actually, because of the existence of quasidegenerated ground states, κ^{IC} around the IC-AF phase boundary as well as near the triple point seems to be considerably large compared with that expected from the calculated $J'_{\text{effect}}(q(T,H))/T$. Although such factors should be included to explain the $H_{\|c}$-T behavior of κ^{IC} consistently, our simple picture explains well why the inverse correlation length along the a^* direction increases as the propagation wave number along the b^* direction approaches 1/2.

3. Appearance of AF domains originated from 2D character

As seen in the $(h\ 1/2\ 0)$ scan shown in Fig. 14(a), in the AF phase we observed unreported small peaks at $(h\ k\ 0)$ with $h,k=$ half-odd integer in addition to the AF peaks at $(h\ k\ 0)$ with $h=$ integer, $k=$ half-odd integer; we call these unreported peaks AF2 peaks. The AF2 peak has the same functional form as that of the main AF peak. As shown in Figs. 15(a) and 15(c), the ratio of both intensities is nearly temperature and magnetic-field independent and the AF2 peak coexists *only* with the AF peak. No other magnetic peak such as $(1/2\ q\ 0)$ with $q\neq 1/2$ was detected in the b^* direction. As shown in Figs. 15(b) and 15(d), κ^{AF2} exceeds κ^{AF} at all the measuring temperatures and magnetic fields, although no observable difference was detected in W_b.

In order to assign the AF2 reflections, we consider two magnetic models: one is the magnetic model yielding both AF and AF2 reflections simultaneously, with magnetic unit cell doubling of the chemical unit cell along both a and b axes; another is the domain model that magnetic structures with magnetic unit cell doubling of the chemical unit cell along both a and b axes coexist with the AF structure of Fig. 3(b) over the crystal. However, the difference between κ^{AF} and κ^{AF2} obviously indicates that two AF and AF2 reflections must come from different magnetic structures and the latter domain model is most likely in $CoNb_2O_6$. Taking account of the Ising character of Co^{2+} spin, both $AF2^+$ and $AF2^-$ structures of Fig. 3(c) are considered to coexist with the AF structure of Fig. 3(b) in the AF phase. Such identification of the magnetic structure is consistent with a recent magnetic structural analysis on isomorphous compounds $FeNb_2O_6$ and $NiNb_2O_6$ by Heid *et al.*[9] Nevertheless, the existence of such magnetic domains in $CoNb_2O_6$ was not reported in their neutron diffraction measurements on $CoNb_2O_6$.[8]

Table I shows the volume fraction of the AF, $AF2^+$, and $AF2^-$ structures for two different single crystals of $CoNb_2O_6$.[21] In both single crystals, the volume fraction of the AF structure is dominant and reproducible for any cooling cycle. The volume fraction differs from sample to sample, confirming the domain model in $CoNb_2O_6$.

As shown in Fig. 3(c), since in the $AF2^{\pm}$ structures the exchange field at the apex site from the base sites through J_2 cancels exactly, it is expected that the 2D magnetic sheets stack along the a axis through the weak interchain interaction J_3 as in the AF structure. However, the $AF2^{\pm}$ structures suggest that J_3 is antiferromagnetic, while the AF structure suggests that J_3 is ferromagnetic. The discrepancy in sign of J_3 indicates the existence of an inhomogeneity in the coupling constant J_3 over the crystal. Taking account of the sample dependence and reproducibility of the volume fraction, such an inhomogeneity might result from a crystal imperfection or a surface effect as suggested in $FeNb_2O_6$ and $NiNb_2O_6$.[9] Such a difference in the coupling constant J_3 causes the different magnitude of the inverse correlation length in the a^* direction for the AF and $AF2^{\pm}$ structures as shown in Figs. 15(b) and 15(d).

As described above, the $AF2^{\pm}$ structures coexist only with the AF structure. When the system goes into the IC state where the exchange field through J_2 is not canceled exactly, the $AF2^{\pm}$ domains disappear. These facts signify that the weak interchain interaction J_3 along the a axis shows

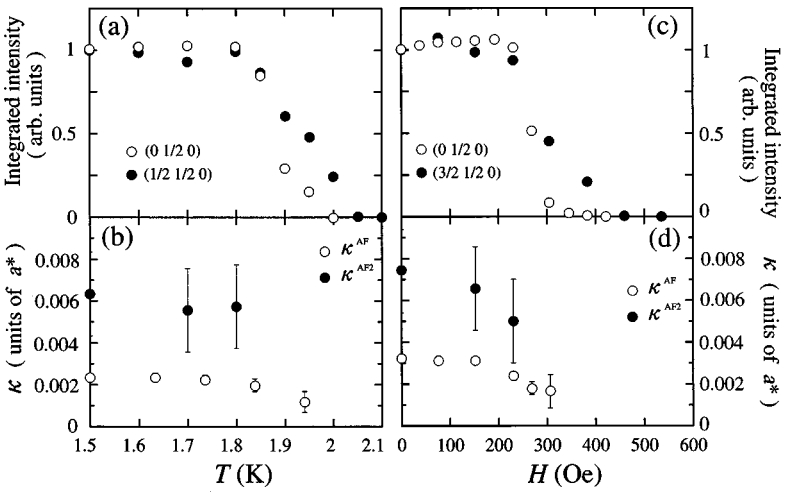

FIG. 15. Temperature dependence of (a) integrated intensities and (b) κ, for the AF and AF2 reflections in zero field. The magnetic-field dependence of (c) integrated intensities and (d) κ, for the AF and AF2 reflections at $T=1.5$ K.

up only in the AF phase where the exchange field at the apex site from the base sites cancels exactly. This supports our finding described in Sec. III E 2 that the difference in the magnitude of the base site spins controls the magnetic correlations along the a axis.

IV. RESULTS AND DISCUSSION FOR $NiNb_2O_6$

In Fig. 14(b), we show the scattering profile of the (h 1/2 0) scan at $T=1.5$ K in zero field. In addition to strong AF peaks at $h=$integer, we observed small AF2 peaks at $h=$half-odd integer as in $CoNb_2O_6$. With increasing temperature, both AF and AF2 intensities gradually decrease, keeping a ratio of both intensities, and disappear at $T_N=5.9\pm0.2$ K, being consistent with a powder neutron diffraction study.[9] However, in contrast to the anomalous broadening of the scattering profile in $CoNb_2O_6$, both AF and AF2 peaks in the a^* and b^* directions are resolution limited at all measuring temperatures. This indicates that $NiNb_2O_6$ exhibits a *true* 3D long-range antiferromagnetism below T_N.

Assuming that the AF and AF2$^{\pm}$ structures shown in Figs. 3(b) and 3(c) are formed below T_N, the volume fraction for each structure is obtained as listed in Table I. In both single crystals the volume fraction of the AF structure largely exceeds that of AF2$^{\pm}$ structures in contrast to the powder results:[9] AF (21%) and AF2$^{\pm}$ (79%). The dominance of the AF structure in the single crystals agrees with the neutron diffraction results on $FeNb_2O_6$ where the AF2$^{\pm}$ domains almost disappear in a single crystal due to fewer surface effects.[9] In addition, the sample dependence of the volume fraction surely confirms that two AF and AF2 reflections originate from different magnetic structures. Noted that using exchange parameters J_1 (~-0.94 K) and J_2 (~0.46 K) estimated by the critical fields[9] in the magnetization process, our isosceles triangular lattice model predicts an appearance of the IC state with $q\sim0.464$ at T_N. Within our experimental accuracy, no such IC state was detected.

TABLE I. Volume fraction of the AF and AF2$^{\pm}$ structures for single crystals of $CoNb_2O_6$ and $NiNb_2O_6$. An equal magnitude of the magnetic moment for all the magnetic structures and an equal volume fraction of the AF2$^{\pm}$ structures were assumed.

	AF (%)	AF2$^+$ (%)	AF2$^-$ (%)
Sample A_{Co}	99.2	0.4	0.4
Sample B_{Co}	97.1	1.45	1.45
Sample A_{Ni}	91.8	4.1	4.1
Sample B_{Ni}	85.1	7.45	7.45

From our single-crystal neutron scattering results, it was confirmed that the AF2$^{\pm}$ structures coexist with the AF structure below T_N in $NiNb_2O_6$. Therefore, the 2D magnetic sheets consisting of the magnetic chains coupled antiferromagnetically along the b axis are considered to correlate to each other through J_3 as in $CoNb_2O_6$. However, the resolution-limited peak in the a^* direction indicates the absence of a pronounced 2D character below T_N. This might be due to a rather strong interchain coupling J_3 or due to the absence of the higher-temperature IC phase because it is expected that the first-order IC-AF phase transition accompanying a nucleation growth easily causes stacking disorder between 2D magnetic sheets as in $CoNb_2O_6$.

V. CONCLUSION

The formation of 3D magnetic ordering has been studied on quasi-1D magnets $CoNb_2O_6$ as well as $NiNb_2O_6$ by neutron scattering measurements down to $T=1.5$ K. The presence of three magnetically ordered phases (AF, IC, and FR) in a quite low-field region below $H_{\|c}\sim500$ Oe in $CoNb_2O_6$ enables us to elucidate the formation of 3D magnetic ordering for most of the ordered phase in detail. Measurements of the deviation of the magnetic Bragg scattering function from the δ function as well as the mean-field calculations revealed interesting magnetic features resulting from the isosceles triangular arrangement of magnetic chains with competing interchain interactions. Below, we itemize our conclusions for $CoNb_2O_6$ and $NiNb_2O_6$.

(1) $CoNb_2O_6$ exhibits a complicated $H_{\|c}$-T magnetic phase diagram which contains three magnetically ordered phases: the AF, IC, and FR phases. The IC region, surrounded by both AF-IC and IC-FR phase boundaries, becomes narrower with decreasing temperature. At a sufficiently low temperature, these boundaries seem to merge, forming a triple point where the AF, IC, and FR phases meet together, although this triple point was not accessible within the present neutron scattering study. Our mean-field calcula-

tions for the isosceles triangular lattice with intrachain ferromagnetic coupling J_0 and interchain antiferromagnetic couplings J_1 and J_2 qualitatively reproduced the $H_{\|c}$-T magnetic phase diagram.

(2) $CoNb_2O_6$ has a high degeneracy of ground states in the IC phase. Approaching the triple point in the IC phase, the number of quasidegenerate ground states with different propagation wave numbers increases. Our mean-field calculations showed that the IC states with different propagation wave numbers have nearly the same free energies in the vicinity of the triple point. Actually, our high-Q resolution neutron scattering measurements revealed a fine structure in the broad IC peak in the b^* direction resulting from an assembly of the IC Bragg peaks with different propagation wave numbers.

(3) In $CoNb_2O_6$, the difference in the magnitude of the base site spins on the isosceles triangular lattice controls the magnetic correlations in the a direction. Particularly, in the AF phase where the exchange field at the apex site from the base site spins cancels exactly, a pronounced 2D character as well as the dependence of the magnetic correlations on the cooling speed from the higher-temperature IC state was clearly observed. Although in $NiNb_2O_6$ the AF structure implies the appearance of a pronounced 2D character as in $CoNb_2O_6$, $NiNb_2O_6$ exhibits a 3D long-range AF ordering below T_N. In both $CoNb_2O_6$ and $NiNb_2O_6$, the interchain interaction J_3 is considered to play a crucial role for the formation of the magnetic ordering along the a axis in the AF state. Indeed, because of the existence of an inhomogeneity in J_3 over the crystal, the magnetic domains in which the stacking of the 2D magnetic sheets along the a axis differs are formed in the AF state.

The diversity of the magnetic formation appearing in $CoNb_2O_6$, in particular, strongly reflects the competing interchain interactions between magnetic chains sitting on the isosceles triangular lattice. If the antiferromagnetic interchain interactions J_1 and J_2 are of the same magnitude, that is, the ratio of interchain interactions $\gamma = J_2/J_1$ is 1.0 (in the case of $CoNb_2O_6$ and $NiNb_2O_6$, $\gamma = J_2 \cos 2\theta_0 / J_1$ because of the two different easy axes), the magnetic system concerned becomes a triangular Ising antiferromagnet with *geometrical frustration*. Geometrical frustration brings a high degeneracy of ground states, and a number of studies have revealed various magnetic features of triangular Ising antiferromagnets.[1] For instance, a quasi-1D Ising antiferromagnet $CsCoCl_3$ with a weak next-nearest-neighbor ferromagnetic interaction in the frustrated triangular lattice exhibits successive phase transitions and a partially disordered phase.[22] Even when such triangular geometrical frustration is partially released, the magnetic property observed might be still characteristic to the frustrated triangular lattice. Recently, the magnetic ordering in the triangular antiferromagnets including partially released geometrical frustration has attracted considerable theoretical[23,24] and experimental[25–27] interest. Experimentally, it was revealed that the XY triangular antiferromagnet $RbMnBr_3$ including an orthorhombic distortion of the exchange bonding with $\gamma \sim 1.28$ provides a very complicated H-T magnetic phase diagram.[26] In view of the inequality in the exchange parameters J_1 (~ -0.0508 K) and $J_2 \cos 2\theta_0$ (~ -0.038 K), $CoNb_2O_6$ also belongs to such triangular antiferromagnets with an orthorhombic distortion. Nevertheless, to our knowledge, we have not heard of Ising magnetic materials showing a surprisingly rich variety of magnetic formation as is found in $CoNb_2O_6$. Taking account of the ratio of $\gamma \sim 0.75$ which is not far from 1.0, a most essential aspect resulting in the interesting magnetic formation in $CoNb_2O_6$ must be the small orthorhombic distortion in the geometrically frustrated triangular lattice. Actually, in the case of $NiNb_2O_6$ with the large orthorhombic distortion of $\gamma \sim -0.23$, fewer competing interchain interactions on the isosceles triangular lattice lead to a simple 3D long-range antiferromagnetism. We believe that the quasi-1D magnet $CoNb_2O_6$ serves as one of the model materials where the triangular geometrical frustration is partially released.

ACKNOWLEDGMENTS

We are grateful to Professor Kiyoichiro Motoya for usage of the SQUID magnetometer at the Science University of Tokyo (Noda campus). We would like to thank Professor Masuo Suzuki for valuable discussions of the mean-field calculations. This work was partly supported by the Science Research Promotion Fund of the Promotion and Mutual Aid Corporation for Private Schools of Japan.

[1] M. F. Collins and O. A. Petrenko, Can. J. Phys. **75**, 605 (1997).
[2] I. Maartense, I. Yaeger, and B. M. Wanklyn, Solid State Commun. **21**, 93 (1977).
[3] W. Scharf, H. Weitzel, I. Yaeger, I. Maartense, and B. M. Wanklyn, J. Magn. Magn. Mater. **13**, 121 (1979).
[4] T. Hanawa, K. Shinkawa, M. Ishikawa, K. Miyatani, K. Saito, and K. Kohn, J. Phys. Soc. Jpn. **63**, 2706 (1994).
[5] S. Mitsuda, K. Hosoya, T. Wada, H. Yoshizawa, T. Hanawa, M. Ishikawa, K. Miyatani, K. Saito, and K. Kohn, J. Phys. Soc. Jpn. **63**, 3568 (1994).
[6] S. Kobayashi, S. Mitsuda, K. Hosoya, H. Yoshizawa, T. Hanawa, M. Ishikawa, K. Miyatani, K. Saito, and K. Kohn, Physica B **213&214**, 176 (1995).
[7] S. Mitsuda, S. Kobayashi, K. Aga, H. Katagiri, H. Yoshizawa, M. Ishikawa, K. Miyatani, and K. Kohn, J. Phys. Soc. Jpn. **64**, 2325 (1995).
[8] C. Heid, H. Weitzel, P. Burlet, M. Bonnet, W. Gonschorek, T. Vogt, J. Norwig, and H. Fuess, J. Magn. Magn. Mater. **151**, 123 (1995).
[9] C. Heid, H. Weitzel, F. Bourdarot, R. Calemczuk, T. Vogt, and H. Fuess, J. Phys. C **8**, 10 609 (1996).
[10] B. M. Wanklyn, B. J. Garrard, and G. Garton, Mater. Res. Bull. **11**, 1497 (1976).
[11] S. Mitsuda, J. Miyamoto, H. Katagiri, K. Aga, S. Kobayashi, and K. Kohn (unpublished).
[12] S. Kobayashi, S. Mitsuda, T. Jogetsu, J. Miyamoto, H. Katagiri, and K. Kohn (unpublished).
[13] E. J. Samuelsen, J. Phys. Chem. Solids **35**, 785 (1974); H. Ikeda,

M. T. Hutchings, and M. Suzuki, J. Phys. C **11**, L359 (1978).
[14] J. von Boehm and P. Bak, Phys. Rev. Lett. **42**, 122 (1979).
[15] Because our model does not include the dipolar energy, the absolute values of the exchange parameters are relatively large compared with those in Ref. 8.
[16] R. J. Elliott, Phys. Rev. **124**, 346 (1961).
[17] Owing to the calculations in a finite size the stepwise behavior of a rational $q_{\rm eq}^{\rm MF}$ was observed in the IC phase. On increasing the cell size N up to infinity, more and more states appear between IC states and a quasicontinuous H^*-T^* variation of $q_{\rm eq}^{\rm MF}$ may be seen in the IC phase.
[18] T. Honma, H. Amitsuka, S. Yasunami, K. Tenya, T. Sakakibara, H. Mitamura, T. Goto, G. Kido, S. Kawarazaki, Y. Miyako, K. Sugiyama, and M. Date, J. Phys. Soc. Jpn. **67**, 1017 (1998).
[19] R. J. Birgeneau, H. J. Guggenheim, and G. Shirane, Phys. Rev. Lett. **22**, 720 (1969).
[20] M. Steiner, J. Villain, and C. G. Windsor, Adv. Phys. **25**, 87 (1976).
[21] Since there exists a deviation of $S(\mathbf{q})$ from $\delta(\mathbf{q})$, the observed integrated intensity reduced from the true observed integrated intensity where $S(\mathbf{q})$ is exactly $\delta(\mathbf{q})$. Thus, in a magnetic structural analysis, we estimated the true observed integrated intensity using width parameters in the AF phase and directly compared the true one with the calculated integrated intensity.
[22] M. Mekata and K. Adachi, J. Phys. Soc. Jpn. **44**, 806 (1978).
[23] For the *XY* system, see H. Kawamura, Prog. Theor. Phys. Suppl. **101**, 545 (1990); M. L. Plumer, A. Caille, and H. Kawamura, Phys. Rev. B **44**, 4461 (1991); W. Zhang, W. M. Saslow, and M. Gabay, *ibid.* **44**, 5129 (1991); W. Zhang, W. M. Saslow, M. Gabay, and M. Benakli, *ibid.* **48**, 10 204 (1993); M. E. Zhitomirsky, O. A. Petrenko, and L. A. Prozorova, *ibid.* **52**, 3511 (1995); M. E. Zhitomirsky, *ibid.* **54**, 353 (1996).
[24] For the Ising system, see J. Stephenson, J. Math. Phys. **11**, 420 (1970); V. G. Vaks and M. B. Geilikman, Zh. Eksp. Teor. Fiz. **60**, 330 (1971) [Sov. Phys. JETP **33**, 179 (1971)]; J. Doczi-Reger and P. C. Hemmer, Physica A **108**, 531 (1981); I. Peschel, Z. Phys. B **45**, 339 (1982); E. Domany and B. Schaub, Phys. Rev. B **29**, 4095 (1984).
[25] C. J. Glinka, V. J. Minkiewicz, D. E. Cox, and C. P. Khattak, in *Magnetism and Magnetic Materials*, edited by C. D. Graham and J. J. Rhyne, AIP Conf. Proc. No. **10** (AIP, New York, 1973), p. 659.
[26] T. Kato, T. Ishii, Y. Ajiro, T. Asano, and S. Kawano, J. Phys. Soc. Jpn. **62**, 3384 (1993); L. Heller, M. F. Collins, Y. S. Yang, and B. Collier, Phys. Rev. B **49**, 1104 (1994); T. Kato, T. Asano, Y. Ajiro, S. Kawano, T. Ishii, and K. Iio, Physica B **213&214**, 182 (1995).
[27] S. T. Bramwell, S. G. Carling, C. J. Harding, K. D. M. Harris, B. M. Kariuki, L. Nixon, and I. P. Parkin, J. Phys. C **8**, L123 (1996); H. Serrano-Gonzalez, S. T. Bramwell, K. D. M. Harris, B. M. Kariuki, L. Nixon, I. P. Parkin, and C. Ritter, J. Appl. Phys. **83**, 6314 (1998).